A continuous lithium atomic beam source for cryogenic apparatus

Brady Stoll

In partial requirement for Dean's Scholar's Honors Degree in Physics
and Plan II Honors Program

University of Texas at Austin
Department of Physics

Dr. Daniel Heinzen
Supervising Professor

Date

Dr. Greg Sitz
Honors Advisor in Physics

Date

Abstract

We have created an atomic beam source of lithium atoms for use in a cryogenic environment. This beam source is expected to provide a flux of 10^{18} atoms/s. The main features of this source are a reservoir chamber of solid lithium heated with heater wire, creating a lithium gas that travels down an ohmically heated tube and exits as an effusive beam. That beam is directed at a cold supersonic jet of helium. As lithium atoms enter the helium gas they rapidly thermalize and become entrained. The design challenges faced included directing the heat load away from the cold elements of the cryogenic chamber, obtaining the correct temperatures to provide the desired flux, and measuring the beam as it exited the reservoir. Through the use of laser induced fluorescence, we believe we have observed capture of lithium by the helium jet. Such a beam source can be used to form an intense cold atom source with the potential future application of serving as a pump source for an atom laser.

Acknowledgements

I would like to thank Michael Borysow and Professor Daniel Heinzen for their assistance with the experiments and work described here. Their help in conducting the experiments and answering all of my questions was invaluable.

Also, I extend many thanks to the mechanics working in the machine shop, particularly Jack. All of their help in creating the parts required for our source was invaluable; we literally would not have been able to make this without them. I would also like to thank the University of Texas Physics Department for the laboratory space provided, allowing this experiment to be conducted.

I am very grateful for my family who continually encourages me and helps me to achieve so many things.

Finally I would like to thank my friends, for still being my friends when all I did for about six months was talk about this thesis, and for at least pretending that they were interested.

Contents

List of Figures

List of Tables

Chapter 1

Introduction

Cold atom physics is currently an area of much research as new physical phenomena are investigated at low temperatures. Experiments such as the potential applications of atom optics and the discovery of Bose-Einstein condensates require large numbers of cold atoms [1]. Being able to effectively and efficiently slow and trap cold atoms and molecules will allow for easier examination of the physics of very cold particles.

We propose to make an intense source of cold atoms. Such a source will be able to produce a beam of cold atoms that can be trapped in a magnetic ring for use in experimentation. Supersonic expansion of helium will be used as an initial coolant for the atoms, followed potentially by laser cooling and finally evaporative cooling. A potential use for this source could be to produce an atom laser, which could be used for precision measurement applications and potentially for practical applications such as atom lithography, which was demonstrated with chromium [2], but has made little progress since then. The main requirement for creating an atom laser is obtaining a source that produces particles at high phase space density, thereby producing the analog of a monochromatic laser beam.

Several types of sources have been utilized to create and trap cold atom gases. The basic design considerations of atomic beam sources consist of decelerating and cooling the beam and then trapping the atoms [3]. There are three main techniques used to slow and cool atoms and

molecules: laser cooling, stark deceleration, and buffer-gas cooling.

Laser cooling consists of two common techniques, the creation of a magneto-optical trap and Zeeman slowing. The capture of up to 10^{10} atoms at temperatures in the micro-Kelvin range has been demonstrated. This was done using lasers to first optically trap and cool a gas before loading that gas into a magnetostatic trap. This technique allowed for much colder temperatures to be achieved [4, 5]. There has been little improvement in this technique in recent years.

Another common type of laser cooling is Zeeman slowing. This technique utilizes radiation pressure from resonant radiation to slow the atoms. Spatially-varying Zeeman shifts are used to compensate for the changing Doppler shift as the atoms slow. In addition, an atomic collimator can be used to collect atoms, and an optical molasses to slow the transverse velocities of the atoms. Both of these increase the percentage of trapped atoms in the source. This set-up led to trapping of a total flux of 3.1×10^{12} atoms/sec, one of the highest seen [6]. This source is limited, however, in the types of particles that can be trapped; the excitation structures of molecules and some atoms are too complicated to be trapped by this method.

Stark deceleration utilizes the Stark effect, whereby particles with electric dipole moments feel a force in a varying electric field, to slow particles. Time-varying inhomogeneous electric fields are used to slow a cooled beam, which can then be loaded into an electrostatic trap. Trapping of state-selected ammonia molecules with a density of 10^6 cm^3 in a volume of 0.25 cm^3 at temperatures below 0.35 K was demonstrated [7]. The benefit of this type of source is that it is able to cool and trap dipolar molecules, thus expanding the types of molecules available for experimentation. A magnetic variation of this technique has also been developed [8]

A final method of cooling atoms and molecules is the buffer-gas method. This method utilizes elastic collisions between atoms of a thermal beam with a cold helium buffer gas. These collisions reduce the temperature of the beam to the temperature of the buffer gas, roughly 240 mK. This technique can trap 10^{12} particles [9]. Many types of atoms and molecules can be used in this source type, making it a very versatile method of cooling. Recently, a method similar to this used hydrodynamic enhancement to produce a flux of 3×10^{12} atoms/sec [10].

Cold atom sources have only development slowly in increasing the number of atoms produced. Techniques involving laser cooling are inefficient and are fundamentally limited by the number of photons, 10^5, required to cool a single atom and by re-scattering affects. Techniques such as Stark deceleration have not led to high phase-space densities. This source will hopefully make a substantial leap forward in the flux produced.

The cold atom source proposed in this paper will be able to provide a high flux of cold atoms that can be trapped and used for experimentation. The use of supersonic expansion of a cold helium jet will allow for lower temperatures to be reached with a high flux. Lithium is used because the Li-He cross section as a function of temperature is well known. It also has the benefit of being light, making it easier to later manipulate in a magnetic field for trapping and is convenient to probe or cool with diode laser sources. However, theoretically this type of cooling will not be limited in the type of molecule that can be used, so long as the particles can be heated to a temperature that will provide the appropriate vapor pressure.

The limitations of this source center on the increased difficulties associated with heavier particles. Heavier particles have higher momentum and so will be more likely to exit the helium jet without becoming entrained. Heavier particles would also have a large forward velocity, and therefore would require an additional slowing stage before trapping. In order to account for these changes it may be necessary to have different design parameters, such as the temperature required to reach the necessary vapor pressure, or the nozzle diameter.

Chapter 2

Lithium Source Design and Implementation

2.1. Goals and Considerations of Source

In order to create a beam of continuous lithium as a useful source, certain limitations were placed on the design. Our source must have a high flux of lithium atoms, therefore the exit point must be close to the seeding point of the helium and there can not be significant amounts of heat transfered to the cold elements of the cryogenic chamber.

The next consideration was the flux of lithium required in order to be useful. This was calculated by optimizing the parameters of helium flow and nozzle position in order to obtain the maximum amount of entrained lithium. The flow of lithium is the desired mole fraction of lithium times the flow of helium, $\Phi_{Li} = \eta\Phi_{He}$. A flux of $\Phi_{He} = 10^{20}$ atom/sec is obtainable from the helium source, and assuming a mole fraction of $\eta = 10^{-3}$, our source will require a flux of 10^{17} atoms/sec at optimum. A flux of 10^{18} will therefore be our goal.

The amount of energy needed to operate the source is dominated by the energy required to maintain the temperature of the lithium in spite of black body losses, which will remove significant amounts of heat from the source during its operation. The nature of these black body losses are

described below and account for the majority of the heat loss from the reservoir and long tube, though a small amount of energy will also be required to melt the lithium in the reservoir. With these considerations in mind, any design must be capable of conducting a substantial amount of heat to the lithium in order to maintain the temperatures required.

Our final limitation was the amount of heat that can be transfered to the cold inner chamber. This chamber, maintained at 4 K, should have a heat load of less than 1 W transfered to it by the lithium. The black body radiation from our source, operated at a temperature of approximately 1000 K, is given by Equation 2.1

$$P = \sigma \epsilon A T^4 \tag{2.1}$$

For our source the emissivity of stainless steel, ϵ, is estimated to be 0.25 when clean and approaching 1 when dirty. The temperature is determined by the flux requirement and is relatively constant. In order to minimize the energy transfer to the cold elements of the inner chamber, the area of the lithium nozzle exposed to the 4 K cryogenic elements should be minimized. Another source of heat for the chamber is the condensation of lithium after it exits the source. Given the total flux expected from the source and the latent heat of condensation of lithium, the total energy transfered from the apparatus will be

$$E_{condensation} = \Phi_{Li} L_{vaporization} \tag{2.2}$$

Our expected flux will have a flow rate of 1.2×10^{-5} g/sec and $L_{vap.}$ is 19,600 J/g, giving a rate of energy transfer from condensation of lithium of 0.22 W.

These considerations led to our current design for the lithium source. We believe that it best addresses these concerns by allowing for adjustment of the flux through temperature changes and reduces the heat transfered to the cryogenic elements to manageable levels.

2.2. Design Features

ne main features of our
l by heater wire, a thin
ture radiation shield by
ubes. The temperature
d is thermally anchored
ding the heater wire is
mineral wool insulation to limit heat losses from the reservoir.

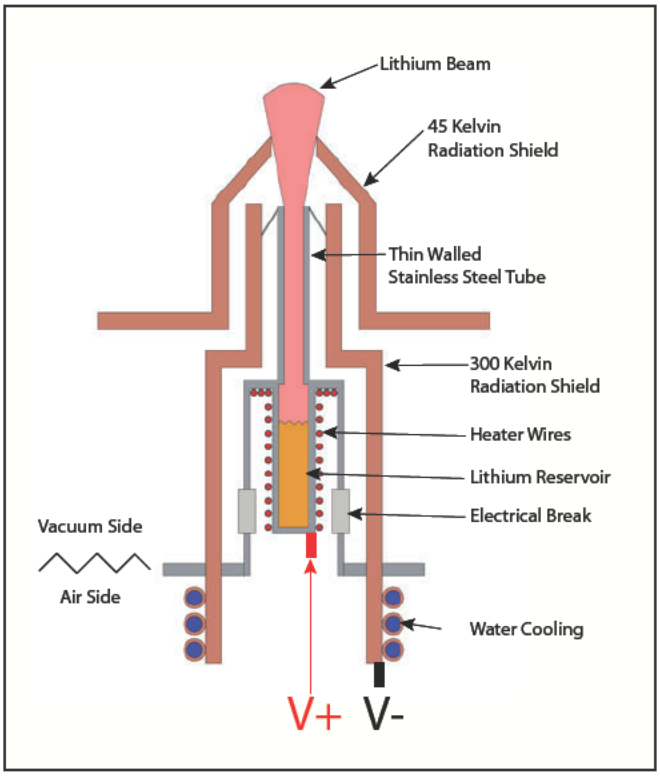

Figure 2.1: Schematic drawing of the lithium source

The purpose of these two shields is to minimize the black body radiation absorbed by the cold elements of the cryogenic chamber. The stainless steel tube is heated ohmically to a temperature of 900 K. The path of the current in this design travels through the lithium reservoir, down the stainless steel tube, and through six wires connecting the tip and the 300 K shield, and

finally continue through the room temperature shield. The positive and negative terminals can be seen in Figure 2.1. The resistance of the lithium source can be calculated straightforwardly from Equation 2.3.

$$R = \frac{l\rho}{A} \tag{2.3}$$

The total resistance of the source with respect to ohmic heating can be seen as four resistors in series: the reservoir, tube, wires, and shield. The resistivity of copper is 1.68×10^{-8} Ω/m at 20 °C and of stainless steel is 11.3×10^{-7} Ω/m at 1000 °C [12, 13]. With the specifications of our design, this will give a resistance of 0.1 Ω. A current of approximately 36 A is run through the oven, providing a power of 130 W to the device.

In addition we used heater wires to increase the temperature of the reservoir. We wrapped the reservoir in heater wire, which provides 300 W of power at 115 V, and created a small disk of heater wire, which provides 700 W at 115 V, to place at the connection of the reservoir and the stainless steel tube. We operated these heaters at 12-15 % of the maximum voltage, so only a fraction of this total power was used. This additional heat allows more accurate control of the temperature of both the lithium and other elements of the design by providing more degrees of freedom in the heating.

The effectiveness of the heater wires and their impact on each other was tested first without ohmic heating or lithium in the reservoir. The temperature dependence of applied voltage in each of the heater wires can be seen in Table 2.1. Temperatures were measured by two thermocouples cemented to the side of the reservoir and disk connecting reservoir and stainless steel tube. The two heater wires worked together to heat the reservoir, as can be seen by the increase in temperature of one heater when the voltage was increased in the other. Thus our ideal temperatures were found by utilizing the heaters in conjunction with each other rather than testing each separately.

We determined the ideal temperature of the lithium in the reservoir based on the vapor pressure requirements at the exit point. The difference in vapor pressure between the tip and the

Voltage vs Temperature of Heater Wire			
$V_{reservoir}$(V)	$T_{reservoir}$ (°C)	V_{disk} (V)	T_{disk} (°C)
0	25	0	25
42	231	0	68
56	384	0	123
77	592	0	198
77	600	40	213
77	628	50	220
77	661	60	251
56	696	70	265

Table 2.1: Relationship between the voltage applied to the two heater wires in the lithium source and the temperature of both the reservoir and the inner disk of the source. The heaters were turned on individually, starting with the wire surrounding the reservoir and then the wire around the disk. The temperature of the disk is required to be higher than listed in this figure, and reaches these temperatures with the addition of ohmic heating, as discussed later.

reservoir was calculated according to the equation for laminar flow through a long tube.

Gaseous flow can be categorized as being either molecular or viscous. Molecular flow occurs when the mean free path is equal to or greater than the tube diameter, otherwise the flow is viscous. In this source, the mean free path becomes comparable to the tube diameter only near the exit, placing this source in the viscous regime. Viscous flow can be divided into laminar and turbulent flow. Laminar flow characterizes a fluid that has few interactions between layers, resulting in smooth flow. Turbulent flow is chaotic, with particles that have velocities in multiple directions. The flow regime can be determined by analysis of the Reynolds number, Re, of the lithium in the stainless steel tube. The Reynolds number is the ratio of inertial to viscous forces in a fluid, given by the equation

$$Re = \frac{\rho v L}{\mu} \tag{2.4}$$

where ρ is the density, v is the velocity, L is the characteristic length, typically the diameter of the tube, and μ is the viscosity [14]. For lithium at 1000 K, $\rho = 8.48 \times 10^{-8}$ g/cm^{3}and $\mu = 122 \times 10^{-7}$ Pa/sec [15], and the tube diameter is $L = 0.091$ cm. Therefore, at our desired temperature, the Reynolds number is $Re = 8.4$ and the source operates well into the laminar regime. The formula for determining the laminar flow rate, Q, in a long, thin tube is

$$Q = \frac{\pi d^4 \Delta p}{128 \mu l} \tag{2.5}$$

where d is the diameter of the tube, Δp is the pressure difference, μ the viscosity, and l is the length of the tube.

In order to reach the desired flux of 10^{18} atoms/sec for our specifications, the pressure difference between the reservoir and tip of the source must be 2.29 kPa. This pressure difference is maintained by manipulating the temperature in the reservoir, thereby changing the vapor pressure of the lithium gas. The source reservoir must have a temperature of slightly higher than 1000 K in order to maintain this difference. This flow rate will provide the required flux at a steady rate and can be maintained for nearly 24 hours, supposing that 1 g lithium is added to the reservoir.

In order to address the heat load on the cryogenic apparatus, this design incorporates cold shields to disperse heat before it reaches the 4 K elements. There are two such shields, one anchored to 300 K and one to 45 K. Each shield should be able to dissipate its heat load to the respective reservoirs while maintaining a relatively stable temperature.

The 300 K shield directly surrounds the reservoir and stainless steel tube, as can be seen in Figure 2.1. This shield is thermally anchored to chilled water, which removes the heat due to black body radiation from the hot elements of the oven. Calculated from Equation 2.1, this is a heat load of 44 W for the specifications of this source operating at 1000 K. In addition, the six end wires connecting the stainless steel tube and copper shield both radiate heat and thermally conduct heat from the tube. This contribution is approximately 5.5 W.

The sheath surrounding the entire lithium source is maintained at 45 K. It absorbs a portion of the deposited lithium, and limits the black body radiation directly incident upon the 4 K elements. The amount of black body radiation incident upon this sheath is approximately 1 W, found by integrating Equation 2.1 over the temperature gradient in the length of the 300 K shield. Also, the tip of the lithium source will be radiating onto this surface, providing another

5.5 W. The final source of heat is the deposition, and subsequent condensation, of lithium. This will vary based on the actual dispersion of lithium as it exits the source nozzle, but will be on the order of 1 W.

The heat load on the 4 K elements of the cryogenic apparatus will have similar factors as that on the 45 K shield. Radiation from the 45 K shield onto the 4 K shield is several mW, but the condensation of lithium is much more significant. Condensation energy is assumed to be approximately 1 W but will vary based on the exact distribution of lithium exiting the source.

2.3. Implementation

2.3.1. Testing of Original Design

This design was first tested in a small vacuum chamber to determine if the current and temperature calculations were correct. In order to run the source, the tip of the stainless steel tube must be heated to temperature before the reservoir is heated, to ensure that hot lithium gas does not condense on the cold tip. Therefore, testing that the entire apparatus is performing as expected is important so that once lithium was added no clogs in the tube were created.

All temperature measurements were made with thermocouple wires. These were attached with thermally conductive cement to the tip of the stainless steel tube, to the outside of the 300K shield, to the reservoir next to the heater wire, and to the connection of the reservoir and stainless steel tube. One was also suspended inside the stainless steel tube.

After a seemingly successful temperature trial, however, this design required modification because the tip of the source would suddenly become cold while the reservoir remained hot. Upon inspecting the inside of the tube we noticed that the tube had actually bent and was touching the inner wall of the surrounding tube, creating a short circuit. Thermal expansion, given by Equation 2.6, causes solids to lengthen as their temperature increases.

$$\frac{\Delta L}{L} = \alpha \Delta T \tag{2.6}$$

For stainless steel, α is 16 μm/m K. Our tube length is 16.74 cm and the change in temperature is between 650 and 700 K, giving a total expansion of 0.17 to 0.19 cm.

The tube was constrained at both ends in the original design, so with expansion it began to bend in the middle. Upon touching the sides of the outer tube electrical contact was established and the current was redirected down the sides of the outer tube, rather than through the tip and the six wires connected to it. Our design utilizes ohmic heating as a temperature regulator of this tube, so an electrical shortage caused the tip to cool considerably.

In order to combat this, we first lengthened the six wires connecting the long inner tube to the outer room temperature shield. This allowed the inner tube to expand so that these six wires were taut not at room temperature but at the expanded length of the inner tube. This was met with limited success; the tube reached a temperature of 449 °C at the tip of the tube and 712 °C at the reservoir without lithium added. We suspect that the lower temperature of the tip measurement is due in part to the cement used to fix the thermocouple to the tip of the tube, which is a large black body emitter. The ohmic heating current dependency can be seen in Figure 2.2. This figure shows a linear dependency through the temperatures that we will be

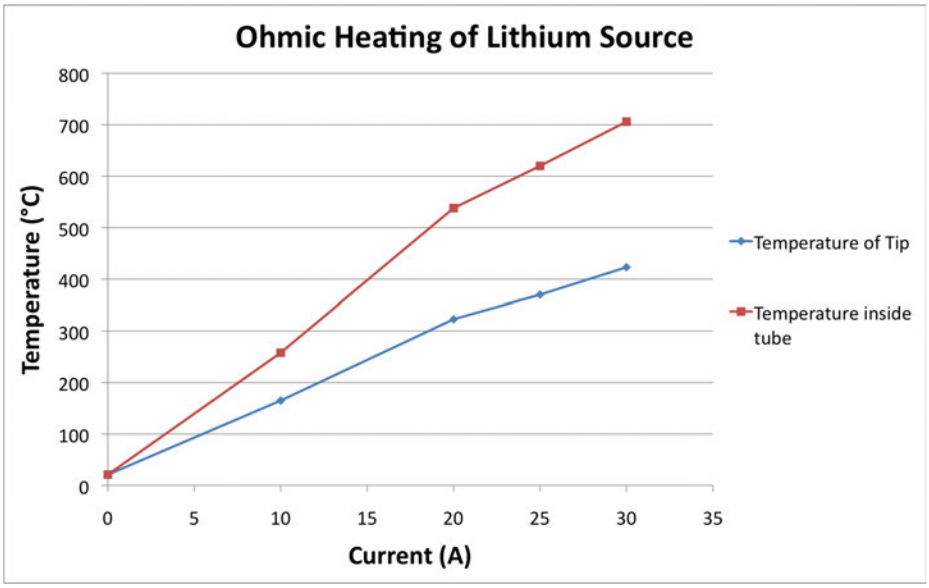

Figure 2.2: Ohmic heating was used to raise the temperature of the long thin tube of the lithium source. This graph displays the current dependence of that temperature, as measured through two thermocouples, one attached to the tip of the source and one placed inside the tube.

using. However, this modification was ultimately unsuccessful. After several heating cycles the tube continued to bend and again shorted to the wall of the 300 K shield. We therefore began more substantial modifications to the lithium source design.

2.3.2. Modifications of Source

In order to remedy the problem of the inner tube expansion we had to redesign certain aspects of the lithium source. The main consideration for this design was allowing expansion of the inner tube within the current design so that an entirely new apparatus was not required. Our first modification of simply lengthening the six connecting wires and de-constraining the source was unsuccessful; the tube reached a higher temperature before bending, but the wires ultimately did not provide sufficient force to keep the tube upright. In order to ensure that the tube would not bend, we anchored the lithium tube and reservoir to four springs, thermally and electrically isolated from both. This provided a downward force on the tube, keeping it straight through the expansion.

We matched the spring constants of these springs such that the length of the expansion of the tube would provide a force on the tube that is slightly larger than the force exerted by atmosphere. Thus, when the tube began to expand the path of least resistance would be to expand downward through the springs rather than to bend. The force of atmosphere is approximately 45 lb, so in order to provide a similar force over the expansion of 0.17 cm, each of the four springs used has a spring constant of $k = 66.2$ lb/cm. The new design can be seen in Figure 2.3

Temperature measurements with the new design were similar to the initial temperature measurements of the first design, but then continued to increase in temperature up to 530 °C, measured on the inside of the long tube. The temperature dependence on the applied current, after modification, can be seen in Figure 2.4. The relationship is very similar to the the dependency before modifications with the addition that the tip of the source was now able to reach temperatures similar to those inside the tube. The new source is able to reach these temperatures repeatedly without mechanical failure, though the tube does still bend slightly when hot. Also,

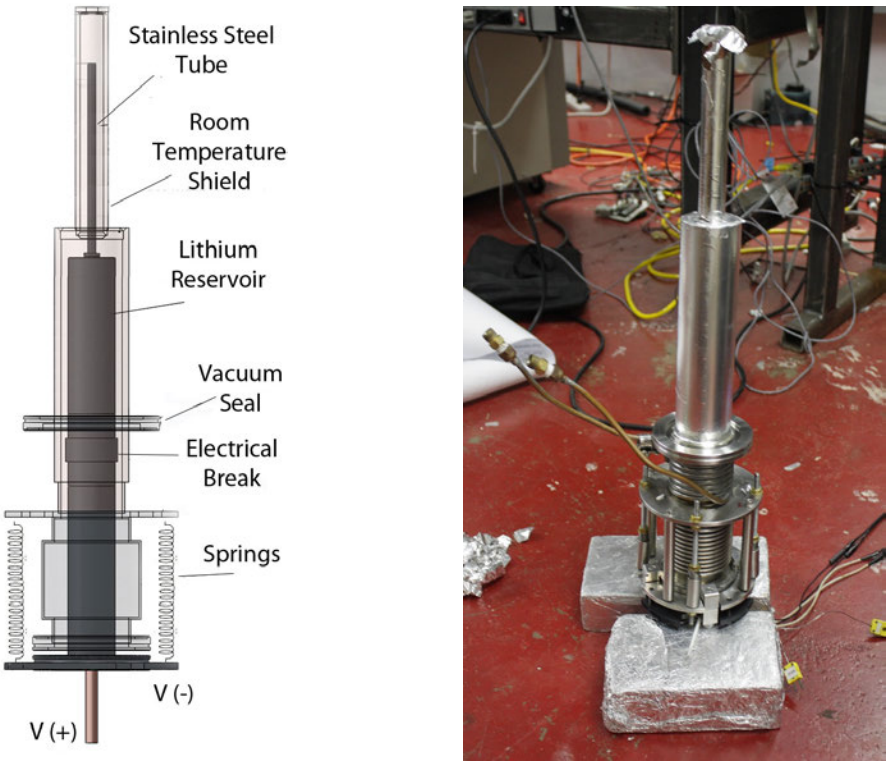

(a) Lithium Source Schematic

(b) Lithium Source Photograph

Figure 2.3: Lithium source design after modifications. The end of the oven was lengthened in order to include four springs, allowing outward expansion of the reservoir and thin tube.

we used smaller amounts of cement to attach the thermocouple to the tip in order to decrease the experimental error in the discrepancy between the measurements of the thermocouple attached to the tip and inside the tube.

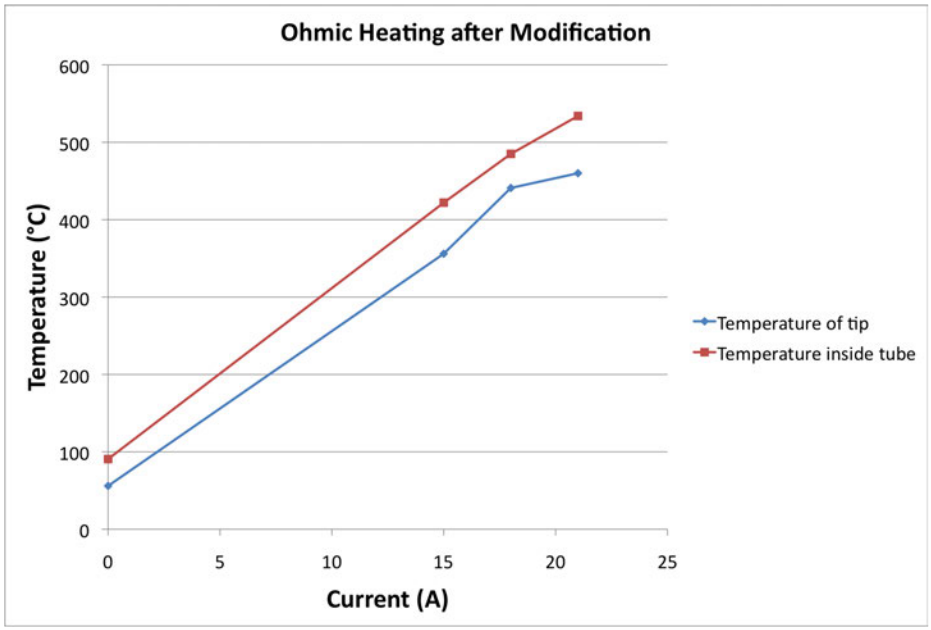

Figure 2.4: Ohmic heating current dependencies of the temperature of the tip of the lithium source after modification of the design

All of the temperature changes of the lithium source can be seen in Table 2.2. This table shows the interactions between each of the heating elements used in the lithium source. The goal of reaching 1000 K, approximately 700 °C, in the reservoir is clearly attainable and should lead to the required vapor pressure. The temperature was also measured on the side of the room temperature shield, approximately 2 cm below the junction of the thin wires with the shield, to determine if the cooling mechanism was performing as expected. The temperature at this point is higher than expected, but not detrimentally so. This will lead to an increase in black body radiation, but the increase should still be dissipated by the 45 K shield.

The success of this new design allowed us to continue measurements of the lithium source. Lithium was added to the reservoir and measurements similar to those above were made. The thermocouple on the tip of the source was removed because it cooled the tip from black body losses, which could be detrimental with lithium in the source, but observations were made of its

Temperature Test of Entire Lithium Source								
$V_{res.}$(V)	$T_{res.}$ (°C)	V_{disk} (V)	T_{disk} (°C)	I_{tip} (A)	V_{tip} (V)	T_{tip} (°C)	$T_{in.}$ (°C)	T_{side} (°C)
0	47	0	47	0	0	24.7	28.5	25
10	118	0	80.4	0	0	29	29	21
30	417	0	293	0	0	33.1	46.2	22.6
45	652	0	514	0	0	56	90.7	31.6
44	676	0	558	15	1.4	356	422	50
44	682	0	568	18	1.5	411	485	59
44	690	0	580	21	17	460	534	66
44	693	10	599	21	1.7	*	530	*
44	712	20	690	21	1.7	449	530	80

Table 2.2: Heating of the lithium source, before lithium was added. Temperature measurements were taken on the lithium reservoir, on the disk connecting the reservoir and long tube, at the tip of the long tube, inside the tube, and on the side of the room temperature shield. As expected, the reservoir reached a temperature higher than the tip, and the shield remained at approximately room temperature. * indicates measurement not taken

color. The red appearance of the tip was similar to trials in which the temperature was known, indicating that it remained hot while operating with lithium. The operating conditions of the lithium source with lithium added can be seen in Table 2.3.

Operating Conditions of Lithium Source					
$V_{res.}$(V)	$T_{res.}$ (°C)	V_{disk} (V)	T_{disk} (°C)	I_{tip} (A)	V_{tip} (V)
56	574	10	636	36	3

Table 2.3: Measurements of the voltages applied to the heater wire and the current for ohmic heating of the lithium source used in maintaining required temperatures. Temperatures listed were taken from a single trial run, but are typical of the run conditions.

Chapter 3

Results

3.1. Measurement of Flux

The lithium source will theoretically produce a flux of 10^{18} atoms. This will be measured by analysis of the deposition of lithium onto a window of the vacuum chamber. In order to measure this flux, we will measure the reflectivity of a 670 nm laser on the surface of a window above the lithium source. The change in reflectivity will provide a measurement of the rate of deposition of lithium onto the surface.

The surfaces of the glass window will change from a air-glass-air interface to air-glass-lithium interface. As the lithium source operates it will begin to plate the window with a thin layer of lithium. The transition between the two conditions is accompanied by a change in the reflectance. The total reflectance for thin films, approximately the conditions of lithium plating on a glass window, depends upon the thickness of the film. Lithium has a skin depth of 20 nm for wavelengths of 670 nm of light [16]. Assuming that lithium behaves as a thin film until three skin depths have been deposited, it will at this point appear opaque and further changes will be negligible. Measurement of the time required to reach this steady state condition and comparison of the measured reflectance with expected dependence on thickness of the lithium layer can be used to determine the flow rate of lithium.

We determined the theoretical reflectance for a thin film system. The layers of the system can be seen in Figure 3.1. Both the initial air-glass-air configuration of the window and the air-glass-lithium-air configuration after the window has been plated with lithium can be seen. The

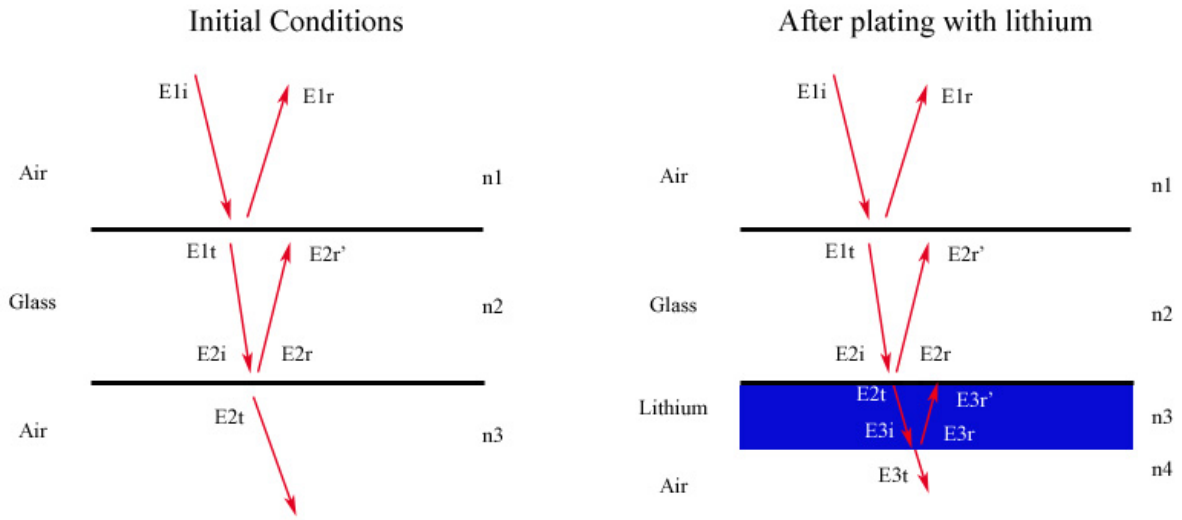

Figure 3.1: The flux of the lithium source is measured based on the reflection of light off of a window. The reflection changes from the air-glass-air interface to air-glass-lithium interface. The reflection and transmission are shown schematically; the angle of incidence is approximately normal when measured.

reflectance of the system can be found by analyzing the boundary conditions for the electric and magnetic fields of the incident light [17]. The tangential components of both the electric and magnetic field must be continuous at each of the three boundaries, leading to the requirement for the electric fields

$$E_1 = E_{1i} + E_{1r} = E_{1t} + E_{2r'} \tag{3.1}$$

$$E_2 = E_{2i} + E_{2r} = E_{2t} + E_{3r'} \tag{3.2}$$

$$E_3 = E_{3i} + E_{3r} = E_{3t} \tag{3.3}$$

For the magnetic field six equations can be generated, but the most important equations for our

purposes are the boundary conditions at the first and last boundary,

$$H_1 = \sqrt{\frac{\epsilon_0}{\mu_0}} n_1 (E_{1i} - E_{1r}) \tag{3.4}$$

$$H_3 = \sqrt{\frac{\epsilon_0}{\mu_0}} n_4 (E_{3t}) \tag{3.5}$$

These equations can be coupled with the phase shift of a wave as it propagates through a medium to correlate the electric components of the wave at each boundary of the same material. The propagation equations are

$$E_{2i} = E_{1t} e^{-ik_0 n_2 d} \tag{3.6}$$

$$E_{2r} = E_{2r'} e^{+ik_0 n_2 d} \tag{3.7}$$

$$E_{3i} = E_{2t} e^{-ik_0 n_3 d} \tag{3.8}$$

$$E_{3r} = E_{3r'} e^{+ik_0 n_3 d} \tag{3.9}$$

In these equations k_0 is the propagation vector, $k = 2\pi/\lambda$ and d is the thickness of the layer. Equations 3.1 - 3.9 can be combined [17] to give a matrix containing the relevant information for the total reflectance and transmittance of the air-glass-air system, Equation 3.10 and for the air-glass-lithium-air system, Equation 3.11.

$$\begin{bmatrix} E_1 \\ H_1 \end{bmatrix} = \begin{bmatrix} \cos(k_0 n_2 d) & \dfrac{i \sin(k_0 n_2 d)}{\sqrt{\frac{\epsilon_0}{\mu_0}} n_2} \\ \sqrt{\frac{\epsilon_0}{\mu_0}} n_2 i \sin(k_0 n_2 d) & \cos(k_0 n_2 d) \end{bmatrix} \begin{bmatrix} E_2 \\ H_2 \end{bmatrix} \tag{3.10}$$

$$\begin{bmatrix} E_1 \\ H_1 \end{bmatrix} = \begin{bmatrix} \cos(k_0 n_2 d) & \dfrac{i \sin(k_0 n_2 d)}{\sqrt{\frac{\epsilon_0}{\mu_0}} n_2} \\ \sqrt{\frac{\epsilon_0}{\mu_0}} n_2 i \sin(k_0 n_2 d) & \cos(k_0 n_2 d) \end{bmatrix} \begin{bmatrix} \cos(k_0 n_3 d) & \dfrac{i \sin(k_0 n_3 d)}{\sqrt{\frac{\epsilon_0}{\mu_0}} n_3} \\ \sqrt{\frac{\epsilon_0}{\mu_0}} n_3 i \sin(k_0 n_3 d) & \cos(k_0 n_3 d) \end{bmatrix} \begin{bmatrix} E_3 \\ H_3 \end{bmatrix} \tag{3.11}$$

The 2×2 matrices above are called M_2 and M_3, based on the same numbering as the

index of refraction, and describe the total interaction of electromagnetic waves in layers 2 and 3 respectively. The matrix M is defined as

$$M = M_2 M_3 = \begin{bmatrix} m_{11} & m_{12} \\ m_{21} & m_{22} \end{bmatrix} \tag{3.12}$$

Combining Equations 3.1, 3.3 - 3.5, 3.11, and 3.12 gives equations for the coefficients of reflection and transmission, $r = E_{1r}/E_{1i}$ and $t = E_{3t}/E_{1i}$, where m_{xy} are the elements of M

$$\begin{bmatrix} 1 + r \\ \sqrt{\frac{\epsilon_0}{\mu_0}} n_1 (1 - r) \end{bmatrix} = \begin{bmatrix} m_{11} t + \sqrt{\frac{\epsilon_0}{\mu_0}} n_4 m_{12} t \\ m_{21} t + \sqrt{\frac{\epsilon_0}{\mu_0}} n_4 m_{22} t \end{bmatrix} \tag{3.13}$$

All of the quantities in Equation 3.13 are known except for d, the thickness of the lithium film. Therefore, solving for r and t in the matrix Equation 3.13 and inserting known quantities such as the indices of refraction of air, glass, and lithium: $0.221 + 2.94\ i$, [18] and thickness of the glass in the window gives a complex equation for the coefficient of reflection, r, as a function of thickness of lithium on the window. Multiplying by the complex conjugate of r gives a measure of the reflectance, R, which can be measured from the fraction of power reflected off of the window. Figure 3.2 shows the theoretical reflectance as a function of thickness of the lithium film for three skin depths worth of lithium.

We have attempted to make this measurement of flux using this method, but were unsuccessful due to possible reduction of the lithium in the reservoir. We are currently cleaning and reinserting lithium into the source in order to make these measurements again.

As lithium exits the source it will have a distribution of $\cos\theta$ with respect to the normal. Integrating this distribution over the angle that will reach the window, approximately 10 % of the lithium exiting the source will reach the window. Using dimensional analysis of the expected flux of the source, the density of condensed lithium, and the volume of lithium required for a depth of three skin depths, the expected time required to completely plate the window is 9-10 min.

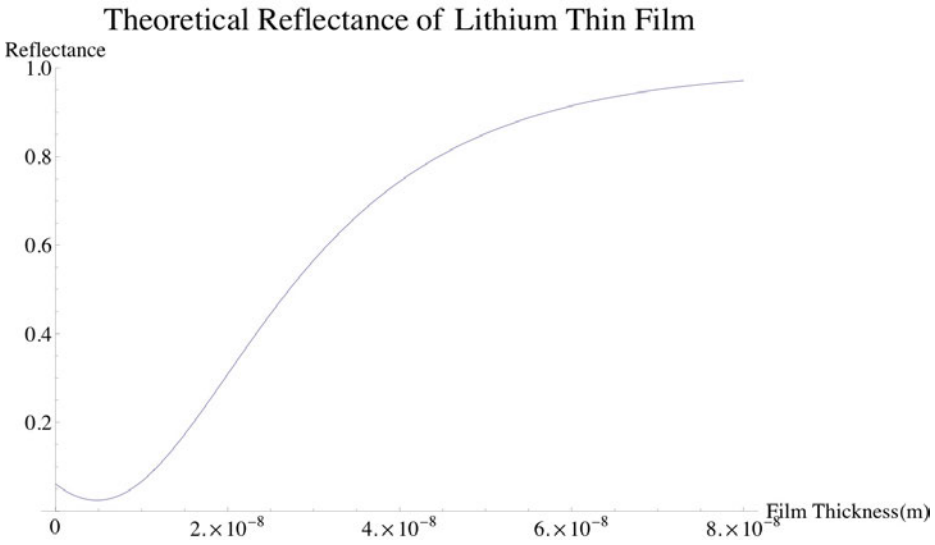

Figure 3.2: Plot showing the theoretical reflectance of lithium film for film thicknesses from zero to three skin depths of lithium

3.2. Heat Load

The ability of the temperature shields to dissipate heat was next determined. The lithium source was inserted into the cryogenic chamber and operated at temperature with lithium. The change in temperature of the cold elements during this time can be seen in Figure 3.3. This demonstrates the effectiveness of the cooling elements at maintaining cold temperatures during the operation of the lithium source; with the lithium source at approximately 700°C, the temperature of the 4 K elements does not increase significantly, indicating success of the design at dissipating heat.

The temperature of the 45 K shield increased more than expected. This is likely due to the higher temperature of the 300 K shield, which can reach temperatures of 350 K as seen in Table 2.2. This increase, however, reached a steady temperature with long operation. The 4 K elements of the apparatus maintain their temperature, indicating that the increases of the 45 K shield are not entirely detrimental to the experiment.

The 4 K elements are cooled with a pulsed tube refrigerator with a 1 W capacity at 4 K. The small increases in the temperature of these elements indicates that the heat load is at least as small as was expected.

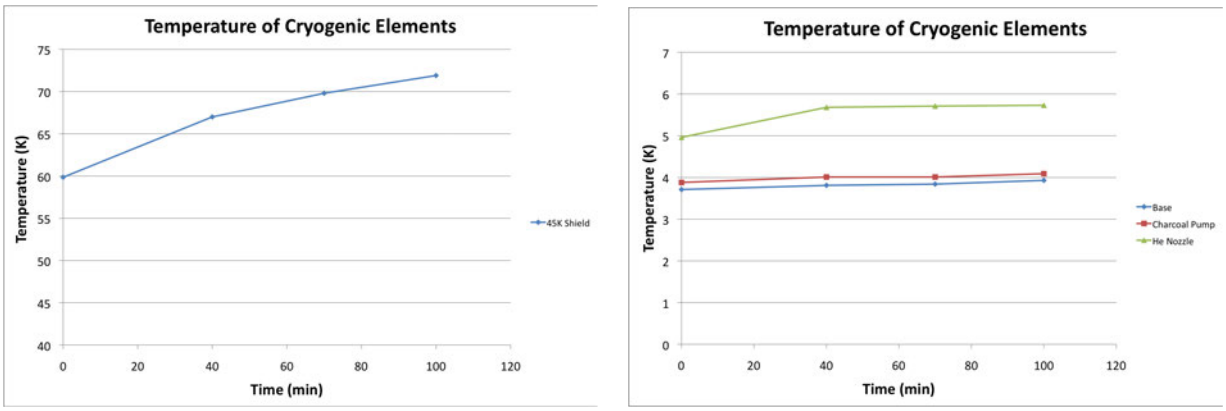

(a) Temperature of 45 K Shield

(b) Temperature of 4 K Elements

Figure 3.3: Temperature measurements of the cryogenic apparatus with the lithium source operating. The temperature of the 45 K shield can be seen to increase in temperature more than the 4 K elements.

In an effort to limit temperatures further, we installed super-insulation on the walls of the cryogenic chamber and around the lithium source. This material has a very low emissivity, helping to reduce black body radiation from the object that it covers. A layer of this material was placed around the room temperature shield of the source to reduce the heat load onto the 45 K shield. The direct effectiveness of this measure is difficult to ascertain, as it was done in conjunction with other modifications to the cryogenic chamber. Between both of these modifications there was a reduction in the base-line temperature of the cryogenic apparatus.

3.3. Capture of Lithium Atoms

The capture of lithium atoms can be seen with the use of laser fluorescence. A laser intersects the lithium beam perpendicularly at the seeding point of the helium jet and excites the lithium atoms, which then release photons that can be measured. The location of this beam can be seen in Figure 3.4.

The frequency of this laser was adjusted from 670.671 nm, tuned to the optical transition of the lithium D lines for ^{7}Li, lithium's most abundant isotope. The relevant transitions in lithium's energy structure can be seen in Figure 3.5. The induced transitions are the D_1: $2S_{1/2} \rightarrow 2P_{1/2}$ and the D_2: $2S_{1/2} \rightarrow 2P_{3/2}$ transitions. Lithium atoms can be red- or blue-shifted with respect

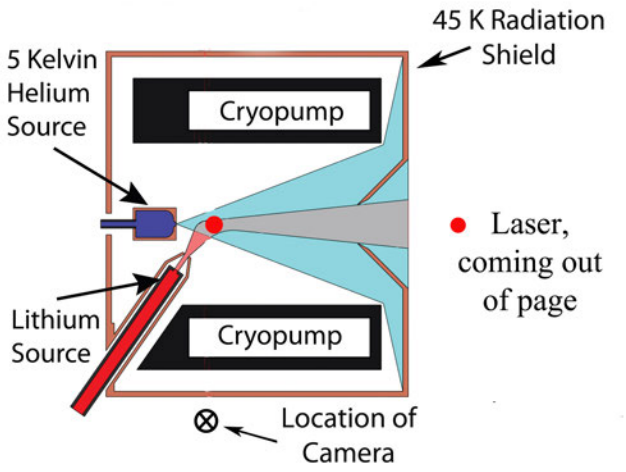

Figure 3.4: Schematic design of fluorescence measurement set up, including lithium source, cold helium jet, laser for inducing fluorescence, and camera location. There is a gap in the middle of the cryopump to allow photo fluorescence to reach the camera, which is pointed in the upwards direction underneath the cryogenic apparatus.

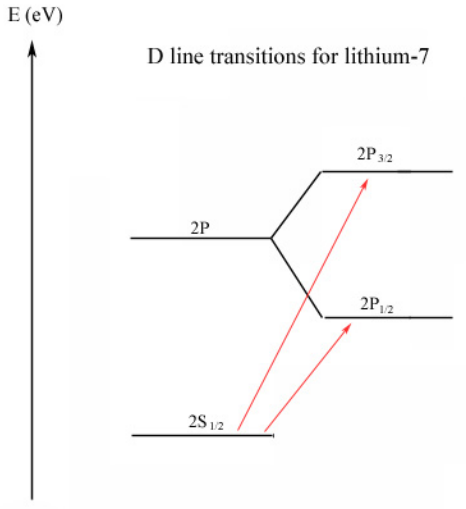

Figure 3.5: Energy levels of lithium. Transitions induced from the $2S_{1/2}$ to the $2P_{1/2}$ and $2P_{3/2}$ levels were measured by laser fluorescence.

to the laser. This shift, given by the Doppler equation

$$\nu = \left(1 - \frac{v}{c}\right) \nu_0 \tag{3.14}$$

changes the frequency, and therefore wavelength of light as seen by the atom. This change is dependent upon the velocity, v of the atom and the initial frequency ν_0 of the light, c is the speed of light. Therefore, atoms of different velocities will be excited by different wavelengths of light. An increase in the range of velocities will have the effect of broadening the distribution of excited states. Alternatively, the angle at which velocities are distributed can change this distribution as well, due to the change in the components of the velocity parallel to the laser beam.

After excitation the atom will decay back to the ground state, releasing a photon as it does so. These photons are recorded by a camera located beneath the seeding point, viewing in the direction perpendicular to the figure. An example of the fluorescence at a particular wavelength can be seen in Figure 3.6. By measuring the intensity of light emitted at these transitions

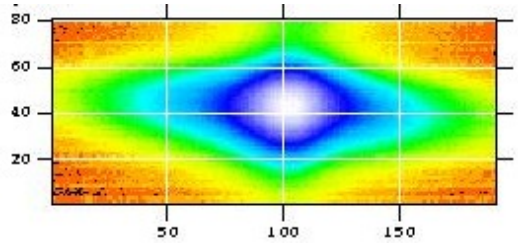

Figure 3.6: Fluorescence of lithium in false color, as seen by the camera located underneath the seeding point. The color scale indicates the intensity of the fluorescence. X and Y scales indicate positioning.

we demonstrated that transitions characteristic of lithium atoms occur. We can determine the temperature of the jet from the velocity distribution plots generated at each point in the gas. As can be seen in Figure 3.7, there are two peaks, showing the two D-line transitions. These peaks have a Gaussian function, characteristic of the velocities of the atoms. The line seen in the figure is the Gaussian function that was fit to the data. These functions were later used for analysis of the data, particularly the width of the peaks. As described above, the width of these peaks is related to the distribution of the velocities of the lithium atoms due to doppler broadening and

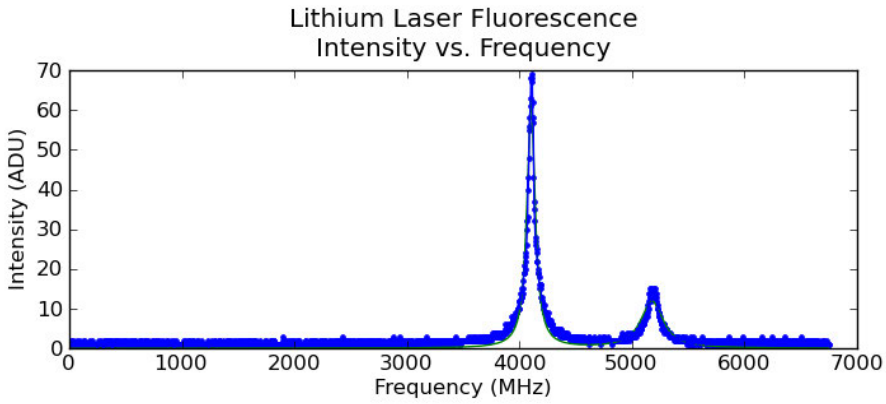

Figure 3.7: Resonance excitations seen in lithium atoms. Frequency scale is the frequency offset, not absolute frequency. The points are actual measurements, the line shows the gaussian function that was fit to the data.

to the angle of the beam's distribution.

We are currently working on determining the velocity distributions of the lithium atoms parallel to the helium jet. Once determined, this information will be used to determine the temperature of the gas. This will be done using the Maxwell-Boltzmann distribution, Equation 3.15.

$$f(\vec{v}) = e^{\frac{-m(\vec{v}-\vec{v}_0)^2}{2kT}} \tag{3.15}$$

where $\vec{v}_0$ is the local jet velocity. The peak velocity can be used to find the temperature from the equation for the root mean square velocity

$$v_{rms} = \sqrt{\frac{3kT}{m}} \tag{3.16}$$

The Maxwell-Boltzmann distribution gives a measure of only the velocity component in the direction of the laser. The lithium atoms will be traveling at an angle θ with respect to the laser, therefore the line width of the data we have currently obtained provides a more direct measurement of the angle of distribution of the atoms. We plan to use this information to extrapolate the total velocity of the gas.

The area of the seeding point was divided into smaller sections based on the images from the camera, Figure 3.6, each 1 pixel by 1 pixel. Each of these areas produced a fluorescence plot

like that of Figure 3.7 and each was fitted to a Gaussian function. The width of each of these peaks was plotted in a false color image in Figure 3.8, the location of the pixel are the x and y axes. Larger values of the width were colored more red and smaller values were blue.

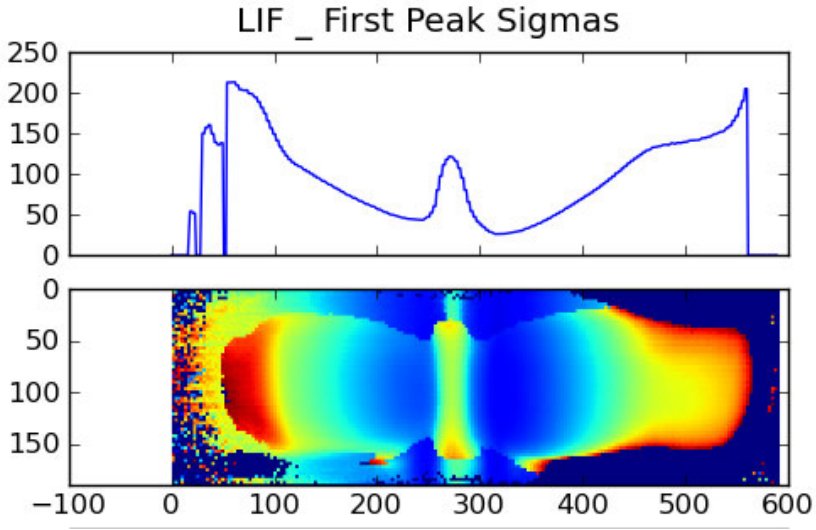

Figure 3.8: Measurements of the spread of the lithium atoms, given by the width of the intensity of excitation, as in Figure 3.7. The x and y axes are positions, measured in pixels. From this information the temperature of the lithium atoms can be found. The top image is a cross section of the total data to better show its structure. The first peak was used for determining the width.

The center peak of the image is wider than is actually present in the data due to poor fitting. We are currently working on determining a better fitting method for this region of the image. A goodness of fit plot was generated to determine how accurately the gaussian model was matching the data. An R^2 value was made for each intensity plot and confirms our suspicions that the inner peak is due to poor modeling rather than an actual phenomena. These R^2 values were found for each gaussian function and were also plotted according to pixel location. The results can be seen in Figure 3.9. In this image, pixels were colored black if their R^2 value was less than 0.8 and are brighter white based on an intensity scale for R^2 above 0.8.

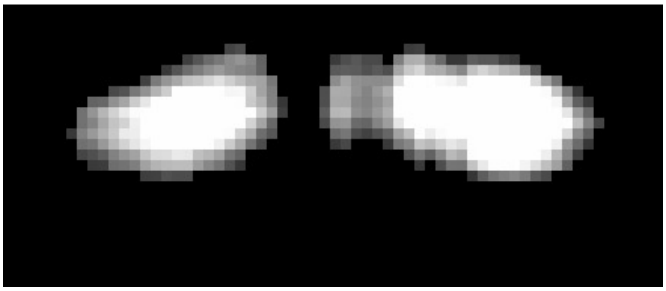

Figure 3.9: R^2 values corresponding to the goodness of fitting for the gaussian model applied to the lithium fluorescence peaks. Black corresponds to a poor fit, either from a lack of fluorescence as seen around the edges, or from poor performance of the fitting algorithm, as seen in the center. This picture is from data similar to, though not the same as, data in Figure 3.8. The phenomena was seen in every trial made and so a qualitative comparison can be made.

Chapter 4

Discussion

Our proposed lithium source appears to be performing as expected thus far. The goal temperature of the lithium source was reached, and lithium was seen to exit the source into the cryogenic chamber, as can be seen in Figures 3.7 and 3.6. The presence of lithium indicates that the calculations made to determine the vapor pressure of lithium and its effect on the production of lithium was correct to at least the first order. Further confirmation of this prediction will be made by the measurement of the flux of lithium, which is currently taking place but has not yet produced results.

In addition, the dissipation of heat by the thermal shields can be improved upon, but is sufficient for further testing of the lithium source and subsequent processes. The source will next be utilized as part of the larger experimental design to produce a cold atom source. Further cooling of the lithium and entrapment of the particles will verify the ability of this new cold atom source to perform as desired.

4.1. Entire Apparatus

Given the continued success of this source, a collimated beam of lithium will be produced that can be trapped in a magnetic storage ring. The lithium, after exiting the lithium source, will

An Intense Cold Atom Source

Michael Borysow*, Travis Briles, Brady Stoll, Daniel Heinzen
Department of Physics, The University of Texas at Austin, Austin, TX 78712
*mborysow@physics.utexas.edu

ntinuous post-nozzle injection of
spects of seeded supersonic jet
cs.[5,6] We expect the brightness of
be achieved by laser-cooling. A

ance predictions. The design
hielded lithium source, and a
nents.

matic of the process can also be

n a nozzle and expands
several milliKelvin in the moving

ined.

ing.

ess of the extracted lithium beam

for the experiment
s 1 and 2. These calculations

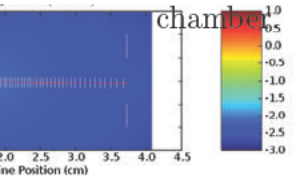

ve is the simulated average path of
e jet having a given a par icular initial
ks represent collisions with helium
color represents he local temperature
g_{10} scale. The trajectory is calculated
model.

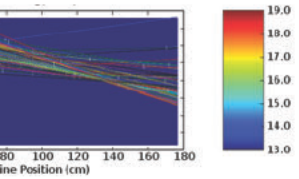

hows trajectories of individual li hium
er as they pass through the field of
e hash marks indicate collision events
particle's flight is modelled using
o methods.

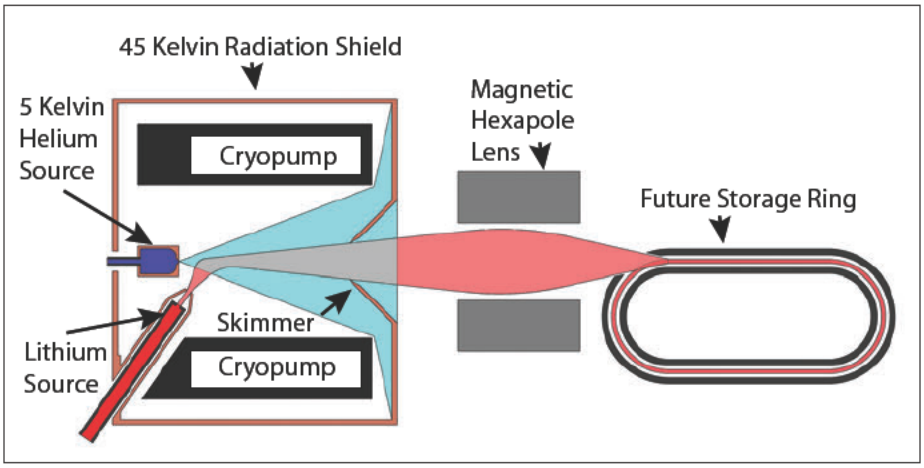

Experiment Schematic

Figure 4.1: Schematic diagram of the entire apparatus, including lithium source, helium jet, cryogenic pumps, skimmer, magnetic hexapole, and magnetic storage ring

We demonstrated that the potential for this type of cold atom source is possible with the successful seeding of the helium jet while maintaining temperatures of 4 K in the cryogenic chamber.

Materials and Methods

1. Helium Jet Source

Helium is delivered to the nozzle from a room temperature cylinder. In order to precool it to the required 5 Kelvin, it is passed through a long copper tube that is thermally anchored to the cold stages. To ensure the helium gas reaches the required temperature, the thermally anchored portions of the tube are helically wound to areas having a good conductive path. The 5 Kelvin thermal anchor of the helium source can be seen in figure 3 to the right. After passing through the tubing, the helium enters a small reservoir and is allowed to escape through the nozzle.

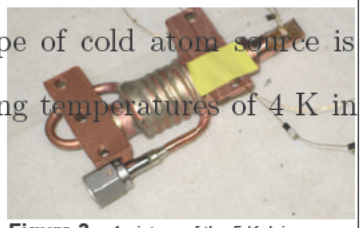

Figure 3. A picture of the 5 Kelvin anchored section of the helium source. The helium is cooled from 45 Kelvin to 5 Kelvin as it passes through the helical coil. A thermal sensor can be seen just atop the nozzle itself.

2. Charcoal Cryosorption Pump

In order to run the experiment in a continuous mode we need a large pumping speed. To that end, we have developed a novel pump for use in jet experiments. The expansion region of the jet is completely surrounded by cryosorption panels slotted into a barrel. These panels can be seen in figure 4. The barrel consists of 60 4"x16" sheets of copper, which are coated with activated coconut charcoal. The entire barrel is cooled to 5 Kelvin. A total of about 2 pounds of charcoal were used, which amounts to an estimated capacity for helium gas of over 100,000 torr-liters. At our intended flux, this provides about 10 hours of run time. Regeneration of the array is possible by heating to 90 Kelvin.

We've made some preliminary measurements of the pump's performance. Utilizing a sniffer tube method, we find that the charcoal pump maintains a helium pressure below 10^{-5} torr with a nozzle flux of 5×10^{19} atoms/s for total gas loads up to 50,000 torr-liters. Further studies of this pump are in progress.

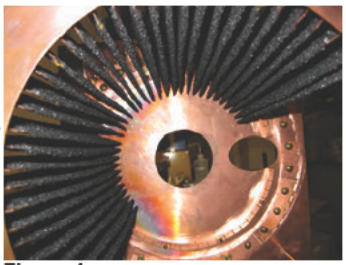

Figure 4. The cryosorp ion pump as seen from he helium nozzle. The inner and outer diameters of the barrel are 8" and 16", respectively. In this image, a number of the panels have been temporarily removed.

2. Lithium Beam

Our source of lithium atoms is
conventional atomic beam oven.
in figure 5. The source consists
stainless steel tube filled with lith
extends outside the vacuum, and
heater wires to 1000 Kelvin. The
extends into vacuum is heated by
the tube to reach the operating te
Extensive heat shielding is requir
radiation reaching cryogenic surfa
due to limited cooling power.

Presently, we have achieved the
tube and are ready to measure th
the beam.

3. Magnetic Hex

After the lithium thermalizes w
extract it from the jet. To that end
magnetic lens to focus the atoms
each 1" thick and 11" in diameter
NdFeB magnets. These magnets
Halbach array,[7] as seen in figure
such a way as to form a nearly pe
lithium atoms due to their magne
directed towards the axis of the le
uninhibited and eventually be pur

The jet itself has just been co
being measured. A preliminary m
seen in figure 6.

Conclusions

We have what we believe is a
atoms. It is particularly interestin
large rates of atoms, high phase
addition, it can potentially be ada

We are currently finishing up w
experiment's components and sh
begin injecting the helium jet with

References

[1] G. Scoles, Atomic and molecular beam
1988).
[2] H. L. Bethlem, G. Berden, and G. Meij
[3] R. E. Grisenti et al., Physical Review L
[4] D. Patterson, and J. M. Doyle, The Jou
[5] E. A. Hinds, and I. G. Hughes, J. Phys
[6] S. Dworski et al., Review of Scientific
[7] K. Halbach, Nuclear Instruments and

Chapter 5

Conclusions

Our research group has proposed a new cold atomic beam source for lithium atoms. After slight modifications of the design, this source withstood initial testing of important variables essential to its later success as an atomic beam source.

As a determination of success, we measured the temperature, heat load, and output of lithium from the lithium source. We found that our source is able to reach the temperatures required for producing lithium vapor pressures as required for seeding into the helium jet; its design incorporates adequate heat shields so that the cold elements of the cryogenic chamber are not exposed to extraordinary amounts of heat, and it produces a beam of lithium atoms as measured by laser fluorescence.

These qualifications indicate that this source design is a valid option for future production of cold atoms, as future testing of the entrainment of lithium by the helium jet and trapping in a magnetic storage ring.

Bibliography

[1] W. Ketterle. *Phys. Review Letters*, **75**, 3969 (1995).

[2] J. J. McClelland, R. E. Scholten, E. Palm and R. Celotta. *Science*, **262**, 877 (1993).

[3] H. Metcalf and P. Straten. *Laser Cooling and Trapping* (Springer, New York, 1999).

[4] C. Monroe, W. Swann, H. Robinson and C. Wieman. *Phys. Review Letters*, **65**, 1571 (1990).

[5] K. E. Gibble, S. Kasapi and S. Chu *Opt. Letters*, **17**, 526 (1992).

[6] C. Slowe, L. Vernac, and L. V. Hau. *Review of Scientific Instruments*, **76**, 103101 (2005).

[7] H. L. Bethlem, G. Berden,F. Crompvoets, R. T. Jongman, A. van Roij, and G. Meijer. *Nature*, **406**, 491 (2000).

[8] E. Narevicius, A. Libson, C. Parthey, I. Chavez, J. Narevicius, U. Even, and M. Raizen. *Phys. Review Letters*, **100**, 093003 (2008).

[9] R. deCarvalho, J. M. Doyle, B. Friedrich, T. Guillet, J. Kim, D. Patterson, and J. D. Weinstein. *European Physical Journal D*, **7**, 289 (1999).

[10] D. Patterson and J. M. Doyle. *J. Chem. Phys.*, **126**, 154307 (2007).

[11] *Lithium*, UCSD. 2002. http://www-ferp.ucsd.edu/LIB/PROPS/PANOS/li.html. 2010.

[12] S. Dobrosavljevic and K. D. Maglic. *International Journal of Thermophysics*, **13**, 57 (1992).

[13] D. E. Gray. *American Institute of Physics Handbook*, 3rd Ed. (McGraw-Hill, New York, 1972).

[14] B. Munson, D. Young, T. Okiishi, *Fundamentals of Fluid Mechanics*, 5th ed. (John Wiley & Sons, Inc, New Jersey, 2006).

[15] A. Ya. Polishchuk, E. E. Shpil'rain, and I. T. Yakubov. *J. Engineering Physics and Thermalphysics*, **38**, 247 (1980).

[16] J. D. McWhirter. *Optics and Lasers in Engineering*, **28**, 305 (1997).

[17] E. Hecht. *Optics* (Pearson Education, Inc., New York, 2002).

[18] M. Rasigni and G. Rasigni. *J. Opt. Soc. Am.*, **67**, 54 (1977).